4. M.Cherkaoui, M.Berveiller, H.Sabar, Micromechanical Modelling of the Martensitic Transformation Induced Plasticity in Austenitic Single Crystals, *Int. J. Plasticity*, (in press)
5. I.Aubert, M.Berveiller, Constrained and Unstable Expansion of Dislocation Loops Using an Invariant Formulation of the Free Energy, to be published, *Mech. of Materials* (1996)
6. J.C.M. Li, Y.T. Chou, The Role of Dislocations in the Flow Stress Grain Size Relationship, *Metal. Trans.*, **1**, (1970), 1145-1158
7. T. Mura, *Micromechanics of defects in solids*, Martinus Nighoff Publisher, (1982)
8. F. David, I.Aubert, X. Lemoine, M.Berveiller, *Computational Mechanics of Materials*, Hambourg, (1997)
9. E.Patoor, M.Berveiller, Cours CISM, to be published, Springer Verlag (1997), 68p
10. E. Gautier, A. Simon, Phase Transformation 87, Ed Lorimer, (1988),285-287

TEXTURE DEVELOPMENT OF ALUMINUM POLYCRYSTALS UNDER FINITE PLASTIC DEFORMATIONS

A. BERTRAM AND T. BÖHLKE

Institut für Mechanik
Otto-von-Guericke-Universität Magdeburg, D-39016 Magdeburg

AND

M. KRASKA

Institut für Mechanik
Technische Universität Berlin, Straße des 17.Juni 135
D-10623 Berlin

1. Introduction

The behavior of polycrystalline aggregates subjected to simple shear deformations has been investigated by several authors (see, for example, [4, 5, 6, 7, 12]). In these works, predictions of both the Taylor model and finite element simulations of the evolution of crystallographic texture and the macroscopic stress-strain response have been compared to experimental data. It is concluded that both models capture the gross features of the observed texture. However, as is well known, the pole densities due to the Taylor model reach higher values than experimental pole densities. It follows from experimental and computational work that the resulting texture can be described in terms of ideal textures (see [4]). The purpose of this paper is to investigate quantitatively the influence of the initial (rolling) texture on the further texture development under simple shear. The particular problem considered here is that of comparing the fibre structure in the initially isotropic and the pretextured aggregate after shearing with regard to the fibre identification, the volume fractions of fibres and the in fibre density distribution. The results are compared with experiments on polycrystalline aluminium samples performed by Williams [1]. For homogenization, the representative volume element technique is compared to the Taylor model.

O. T. Bruhns and E. Stein (eds.),
IUTAM Symposium on Micro- and Macrostructural Aspects of Thermoplasticity, 127–136.

2. Single Crystal Model

Elastic Law. Each grain of the polycrystalline aggregate is assumed to be a single crystal. The model for the single crystalline behavior is based on the assumptions that elastic ranges exist and the corresponding elastic laws are isomorphic [8, 11]. As a result, the current elastic law is given by

$$\mathbf{S} = \mathbf{P}\mathcal{K}_0[\mathbf{P}^{\mathrm{T}}\mathbf{C}\mathbf{P} - \mathbf{I}]\mathbf{P}^{\mathrm{T}}, \tag{1}$$

$\mathbf{S} := \mathbf{F}^{-1}\,\mathbf{T}\,\mathbf{F}^{-\mathrm{T}}$ being the material stress tensor, $\mathbf{F}$ the deformation gradient, $\mathbf{T}$ the Cauchy stress tensor, $\mathbf{C}$ the right Cauchy Green tensor, and $\mathcal{K}_0$ the initial forth order elasticity tensor. $\mathbf{P}$ is an invertible second order tensor, called *plastic transformation*, which is given by the flow rule.

Flow Rule. Plastic deformations in single crystals at room temperature are dominated by slip mechanisms on specific crystallographic planes. In the present work the slip system theory with twelve octahedral slip systems is applied (e.g. [9]). The problem of selecting five active slip systems is avoided by assuming a rate dependent flow rule. As long as the resolved shear stresses $\tau_\alpha = \mathrm{tr}(\mathbf{S}\mathbf{C}\,\mathbf{d}_\alpha \otimes \mathbf{n}^\alpha)$ of all slip systems $(\mathbf{d}_\alpha, \mathbf{n}^\alpha)$ are below the critical ones $\tau_{c\alpha}$, no slip occurs according to Schmid's law, and, thus, $\mathbf{P}$ remains constant. If, however, $|\,\tau_\alpha\,| > \tau_{c\alpha}$, the slip system can be activated and the rate of $\mathbf{P}$ is given by a linear combination of Schmid tensors multiplied by the corresponding slip system shearing rates $\dot{\mu}_\alpha$

$$\dot{\mathbf{P}}\mathbf{P}^{-1} = \begin{cases} \mathbf{0} & \text{if} \,|\,\tau_\alpha\,| \le \tau_{c\alpha}, \\ \sum_\alpha -\dot{\mu}_\alpha \mathbf{d}_\alpha \otimes \mathbf{n}^\alpha & \text{if} \,|\,\tau_\alpha\,| > \tau_{c\alpha}. \end{cases} \tag{2}$$

The slip rate has been chosen as being proportional to the overstress, i.e. $\eta\,\dot{\mu}_\alpha = \mathrm{sign}(\tau_\alpha)(\,|\,\tau_\alpha\,| - \tau_{c\alpha})$.

Hardening. The isotropic hardening on the slip system level is assumed to be governed by the following equation

$$\dot{\tau}_{c\alpha} = \sum_\beta h(\tilde{\mu})\; q_{\alpha\beta}\,|\,\dot{\mu}_\beta\,|\,. \tag{3}$$

The ratio of latent to self hardening is taken as 1.4 so that the matrix elements $q_{\alpha\beta}$ are equal to 1 for $\alpha = \beta$ and 1.4 for $\alpha \neq \beta$. The single slip hardening rate $h(\tilde{\mu})$ depends on the accumulated sum of slips $\tilde{\mu} = \int_0^t \sum_\alpha |\,\dot{\mu}_\alpha\,|\,dt$ and is given by

$$h(\tilde{\mu}) = h_s + (h_0 - h_s)\,\mathrm{sech}^2\left(\frac{h_0 - h_s}{\tau_s - \tau_0}\tilde{\mu}\right). \tag{4}$$

τ_0 and τ_s are the initial and asymptotic values of shear stress, h_0 and h_s the hardening rates [4].

3. Homogenization Procedure

RVE Technique. There are mainly four classical techniques of homogenization corresponding to different kinematic or dynamic assumptions, namely the Taylor model, the Sachs model, self consistent schemes and the representative volume element (RVE) technique. For the latter a boundary value problem is solved for a representative volume of the heterogeneous microstructure. This technique is used in this work because it incorporates interactions of neighboring crystals and fulfills both compatibility and equilibrium condition.

Micro-Macro Transition. The displacement field $\mathbf{u}$ in the aggregate is split into two parts $\mathbf{u} = (\bar{\mathbf{F}} - \mathbf{I})\mathbf{X} + \mathbf{w}$, one corresponding to the mean deformation $\bar{\mathbf{F}}$, the other to a local fluctuating part $\mathbf{w}$. $\mathbf{X}$ is the initial position vector. The Taylor model is contained in the present one by setting $\mathbf{w} = \mathbf{o}$ in the RVE. Assuming the microscopic displacement fluctuations to vanish or be periodic on the boundary of the RVE, the global deformation gradient can be shown to be equal to the mean value of the local deformation gradient taken over the volume in reference placement. A similar expression can be found for the global Cauchy stress. Here the integral has to be taken over the volume in the actual placement (see [3]).

Finite Element Implementation. For the calculation of the stress response due to a given macroscopic deformation process, a three-dimensional nonlinear finite-element approach is used. The RVE is discretized by tetrahedral elements. When $\bar{\mathbf{F}}$ is prescribed, a solution for the actual nodal fluctuations $\mathbf{w}_K$ has to be calculated. Thus, the formulation of the problem in terms of the nodal fluctuations instead of the common nodal displacements is reasonable [13]. For the RVE simulations, periodic boundary displacement fluctuations are imposed.

Uniformly Distributed Random Orientations. A crystal orientation can be represented by the Euler parameters $(q_\kappa) = (n_1 \sin\varphi/2, n_2 \sin\varphi/2, n_3 \sin\varphi/2, \cos\varphi/2)$, with $\mathbf{n}$ and φ being the axis and angle of rotation, respectively. The angular distance φ_{12} between two orientations $\mathbf{q}_1$ and $\mathbf{q}_2$ is given by $cos(\varphi_{12}/2) = \sum_\kappa q_{1\kappa} q_{2\kappa}$. This induces a constant metric on a 3 dimensional unit hyper sphere. Thus the Euler parameters can be considered as components of a 4 dimensional Euclidean unit vector. This provides a simple way of generating uniformly distributed orientations from random numbers in $[-1, 1]$ by choosing random quadruples q_κ with $r := \sqrt{\sum_\kappa q_\kappa^2} \in (0, 1]$ and projecting them to $r = 1$ (Fig. 1). With $\mathbf{q}_I = \sum_{i=1}^3 q_i \mathbf{e}_i$ and $q_R = q_4$ an orientation is obtained in a pure algebraic way: $\mathbf{Q} = 2\mathbf{q}_I \otimes \mathbf{q}_I + (2q_R^2 - 1)\mathbf{I} + 2q_R \mathbf{I} \times \mathbf{q}_I$.

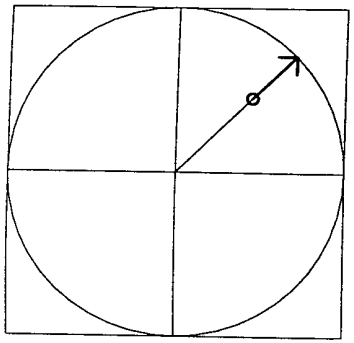

Figure 1. Generation of uniformly distributed points on the surface of a spherical shell.

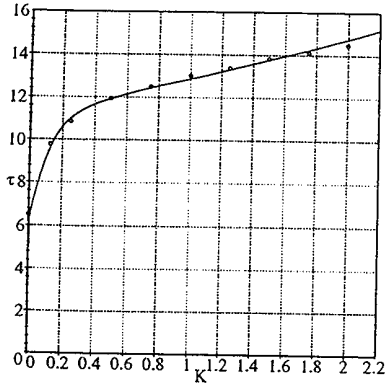

Figure 2. Shear stress vs shear number (τ in 1000 psi).

4. Numerical Example

RVE-Specification. Williams [1] determined the texture produced by simple shear in a rolled polycrystalline sample of aluminium. The sample is sheared perpendicular to the rolling-direction up to a shear magnitude $K = 2.2$ whereas the shear plane normal is collinear to the rolling direction. The amount of thickness reduction and the initial texture is not given in [1]. In the numerical simulations, an RVE with $7 \times 7 \times 7$ nodes is used. The structure contains 1080 tetrahedral elements. A set of 1080 orientations has been generated by the above procedure. The {111} stereographic pole figure of the initial orientation distribution is shown in Fig. 3. The rolling deformation is approximated by the state of plane strain compression with 25% reduction of thickness.

Material Constants. For the numerical simulation the following elastic constants have been used [2]: $E = 63\,\text{GPa}$ (Young's modulus), $G = 28\,\text{GPa}$ (shear modulus), $\nu = 0.36$ (Poisson's ratio). The material parameters of the hardening relation have been calibrated by the stress strain curve given in [1] (see Fig. 2): $\tau_0 = 25\,\text{MPa}$, $\tau_s = 39\,\text{MPa}$, $h_0 = 60\,\text{MPa}$, $h_s = 4.4\,\text{MPa}$. The strain rate and the viscosity are chosen such that the overstress in the global stress-strain curve is lower than 5% of the equilibrium stress.

Shear Texture Description in Terms of Fibres [10]. The {111} pole figure of the texture induced by the plane strain compression (rolling) is given in Fig. 4. Fig. 5 shows the {111} pole figure after subjecting the initially isotropic and the pretextured aggregate to simple shear. It can be seen that the texture development is strongly influenced by the initial texture.

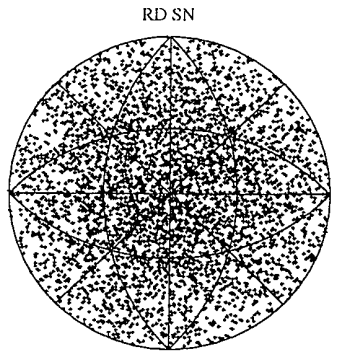

Figure 3. Initial orientation distribution of 1080 grains represented by {111} stereographic pole figure.

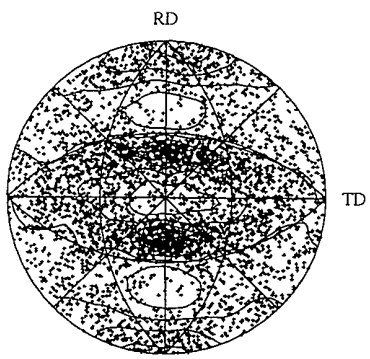

Figure 4. {111} pole figure predicted by an FE-calculation of an plane strain compression test with 25% reduction.

In the case of an initial rolling texture the poles concentrate in regions that correspond to maxima that William determined experimentally. For an initially random distribution the correspondence is less pronounced. When the RVE technique is employed the orientation distribution is principally the same but less sharp as predicted by the Taylor model.

The results of [1] have been compared to simulations using the Taylor model by [4]. The resulting texture is discussed in terms of ideal shear textures, the so called A- and B-fibres. The A-fibre consists of grains with one {111}-pole aligned with the global shear normal (y). For the B-fibre the global shear direction (x) coincides with crystallographic ⟨110⟩-directions. The components of the corresponding rotation tensors are

$$\mathbf{Q}_A = \begin{bmatrix} -\frac{\sqrt{2}}{\sqrt{3}}\sin\alpha & \frac{1}{\sqrt{3}} & -\frac{\sqrt{2}}{\sqrt{3}}\cos\alpha \\ -\frac{1}{\sqrt{2}}\cos\alpha + \frac{1}{\sqrt{6}}\sin\alpha & \frac{1}{\sqrt{3}} & \frac{1}{\sqrt{2}}\sin\alpha + \frac{1}{\sqrt{6}}\cos\alpha \\ \frac{1}{\sqrt{2}}\cos\alpha + \frac{1}{\sqrt{6}}\sin\alpha & \frac{1}{\sqrt{3}} & -\frac{1}{\sqrt{2}}\sin\alpha + \frac{1}{\sqrt{6}}\cos\alpha \end{bmatrix} \mathbf{e}_i \otimes \mathbf{e}_j, \quad (5)$$

$$\mathbf{Q}_B = \begin{bmatrix} 0 & \cos\beta & -\sin\beta \\ -\frac{1}{\sqrt{2}} & \frac{1}{\sqrt{2}}\sin\beta & \frac{1}{\sqrt{2}}\cos\beta \\ \frac{1}{\sqrt{2}} & \frac{1}{\sqrt{2}}\sin\beta & \frac{1}{\sqrt{2}}\cos\beta \end{bmatrix} \mathbf{e}_i \otimes \mathbf{e}_j. \quad (6)$$

Following [4], experimental shear textures contain orientations with $\alpha = -60° \ldots 0°$ in the A-fibre (labelled A_f). The components are concentrated around the position $\alpha = -30°$ and the shear direction is coinciding with ⟨112⟩. The B-fibre has components mainly within $\beta = -55° \ldots 55°$ (B_f).

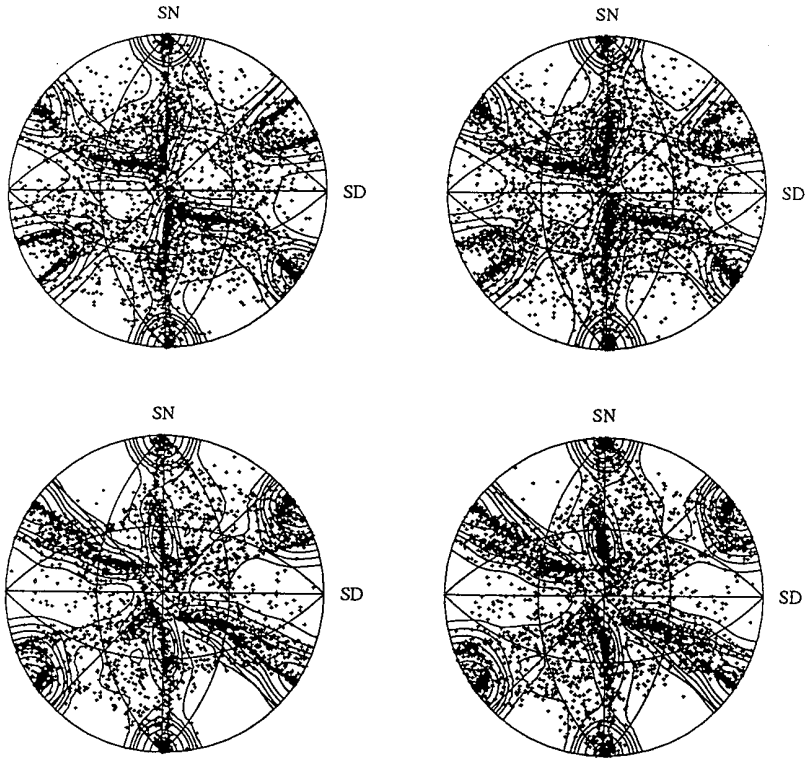

Figure 5. {111} pole figure predicted by subjecting the initially isotropic aggregate (above) and the pretextured aggregate (below) to simple shear (left: Taylor model, right: RVE)

The density is maximal at $\beta = 0°$, the so called C-component. For the description of the pole figures obtained from the pretextured state, an additional fibre is required. Starting from the C-component, such a fibre can be generated by an axis in the mirror-plane of the global shear deformation. The volume fraction of such a fibre depends on the angle φ between x-axis and fibre axis, $\varphi = 0°$ being the B-fibre. Fig. 7 shows the corresponding curves for $K = 2.2$. An orientation is considered to belong to the fibre if it is within a scatter band of 5° around the ideal fibre orientation. The values due to the Taylor model are generally slightly larger than for the RVE. However, this factor is negligible compared to the influence of the initial texture. For initial isotropy, the dominant fibre is B (23% around

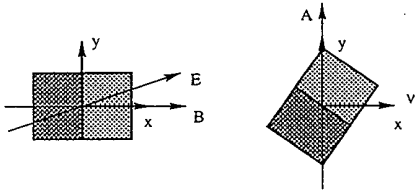

Figure 6. Basic components and fibre axes for A-, B- and E-fibres.

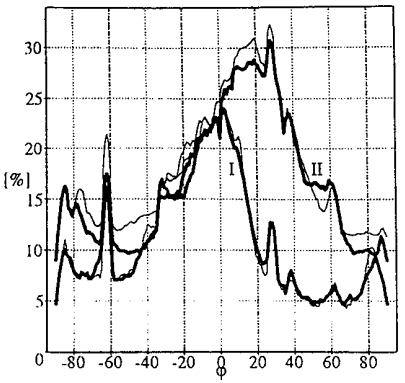

Figure 7. Volume fraction of fibres defined by φ for $K = 2.2$: isotropic (I), pretextured (II), RVE (—), Taylor(–).

$\varphi = 0°$). An initial rolling texture shifts the maximum to 31-33% at $\varphi = 19°$ (furtheron labelled by E-fibre). Their axis coincides with crystallographic (221)-directions. All curves show sharp secondary peaks at $\varphi = -62°$ and $\varphi = 28°$. However, the grains forming these peaks are also contained in the A-fibre, thus no additional fibre is required for their description. Fig. 6 shows the fibre axes and the basic components which are stable components for simple shear [8]. The {111} pole figures of grains within the A-, B- and E-fibre are given in Fig. 8.

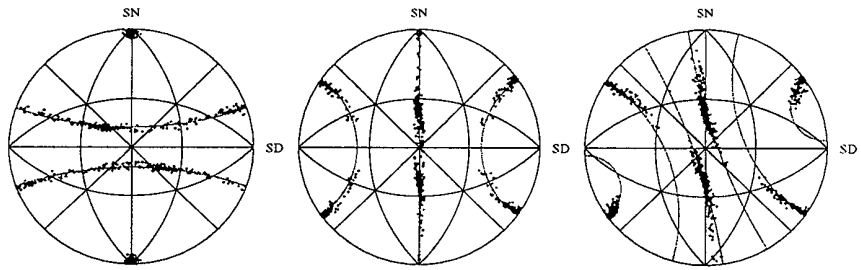

Figure 8. {111} pole figure of grains within the A-, B- and E-fibre (from left to right) for the pretextured and sheared aggregate (RVE simulation).

Volume Fractions of Fibres. The volume fractions of fibres as functions of shear strain are shown in Fig. 9-11(left). The two homogenization techniques principally result in the same amount of fibres, with exception of the

A-fibre for $K > 0.5$. For this fibre the Taylor model predicts a larger volume fraction compared to the RVE technique as remarked in [12]. The initial texture is important for the evolution of volume fractions of the A- and E-fibre whereas the fraction of B-fibre is not affected. The initial texture increases the amount of the A-fibre for $K < 1.75$, that one of the E-fibre for $K > 0.75$. The prestraining shifts the fraction of E-fibre for $K = 2.2$ from 10.26% to 29.32%.

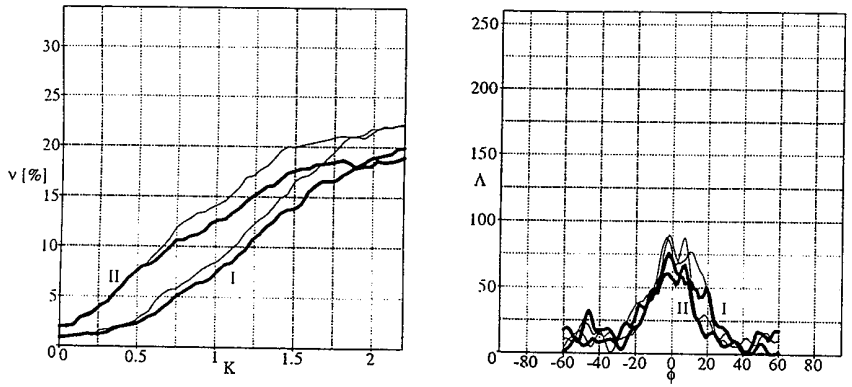

Figure 9. Fraction of grains within the A-fibre vs shear number K (left) and density distribution within the A-fibre (right): isotropic (I), pretextured (II), RVE (—), Taylor(–).

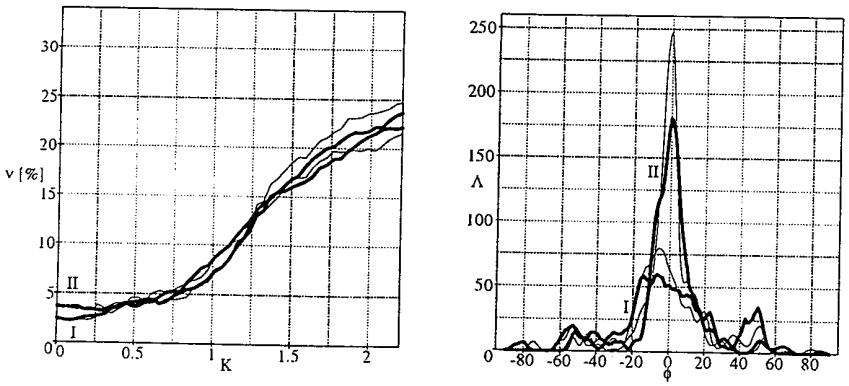

Figure 10. Fraction of grains within the B-fibre vs shear number K (left) and density distribution within the B-fibre (right): isotropic (I), pretextured (II), RVE (—), Taylor(–).

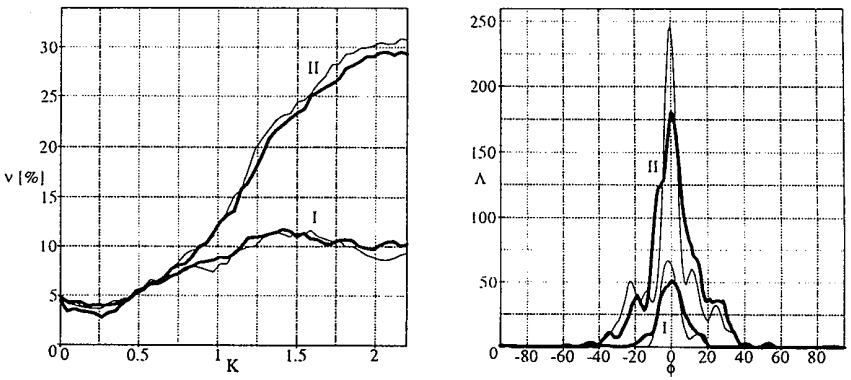

Figure 11. Fraction of grains within the E-fibre vs shear number K (left) and density distribution within the E-fibre (right): isotropic (I), pretextured (II), RVE (—), Taylor(–).

Density Distribution within the Fibres. In order to resolve the angular distribution in the fibres, the orientation density distribution for the corresponding components is examined. The density normalized to the uniform distribution is labelled by Λ. The in-fibre angle (ϕ) is counted from the basic component around the fibre axis in a range corresponding to the symmetry of the crystallographic indices of the fibre axis. The basic component of the A-fibre in the present work corresponds to $\alpha = -30°$ in [4]. For comparability the abscissa ranges of the plots are always $-90° \ldots 90°$. This is acceptable, as the cut off components of the E-fibre are not present in the texture.

In the A-fibre plot the components are concentrated mainly within $-30° \ldots 30°$. As expected from the pole figures, the contents of B- and E-fibres depends strongly on the initial texture. For initial isotropy, the shape of B is similar to that of A, whereas E practically is not present outside the common C-component. When starting from textured state, the most striking feature is the strong C-component. As the overall volume content of B is practically the same, this leads to a reduced width of the in-fibre distribution. The dominance of the E-fibre is due to a considerable density within $-40° \ldots 40°$. The usage of the RVE homogenization method results in a smoothing of the curves, most pronounced in the reduced C-density (from 246 to 180). This reflects the generally more smooth texture obtained by the RVE calculations.

5. Conclusions

A procedure to generate uniformly distributed orientations from random numbers has been introduced and turns out to be a simple way to get large sets of initial orientations. Subjecting the pretextured aggregate to the shear deformation results in improved texture predictions in terms of both the intensity levels and the location of certain texture components. This emphasizes the fact that the texture development is strongly influenced by the initial texture. For initial isotropy the resulting texture can be described in terms of the A- and B-fibres [4]. When starting from textured state the E-fibre is dominant. The RVE homogenization method leads to a smoothing of the density distribution within the fibres. The two homogenization techniques result principally in the same volume fractions of fibres vs shear number with exception of the A-fibre for which the Taylor model predicts a larger volume fraction.

References

1. Williams, O.W. (1962) Shear textures in copper, brass, aluminum, iron and zirconium, *Trans. Met. Soc. AIME* **224**, pp. 129–139
2. Weißmantel, C. and Hamann, C. (1979) *Grundlagen der Festkörperphysik*. Deutscher Verlag der Wissenschaften, Berlin.
3. Krawietz, A. (1986) *Materialtheorie*. Springer–Verlag.
4. Harren, S., Lowe, T.C., Asaro, R.J. and Needleman, A. (1989) Analysis of large-strain shear in rate-dependent face-centred cubic polycrystals: Correlation of micro- and macro-mechanics, *Phil. Trans. R. Soc. Lond. A* **328**, pp. 443–500
5. Harren, S., Asaro, R.J. (1989) Nonuniform deformations in polycrystals and aspects of the validity of the Taylor model, *J. Mech. Phys. Solids* **37**(2), pp. 191–232
6. Bronkhorst, C.A., Kalidindi, S.R. and Anand, L. (1992) Polycrystalline plasticity and the evolution of crystallographic texture in FCC metals, *R. Soc. Lond. A* **341**(3), pp. 443–477
7. Kalidindi, S.R., Bronkhorst, C.A. and Anand, L. (1992) Crystallographic texture evolution in bulk deformation processing of FCC metals, *J. Mech. Phys. Solids* 40(3), pp. 537–569
8. Bertram, A. and Kraska, M. (1995) Determination of finite plastic deformations in single crystals, *Arch. Mech.* **47**(2), pp. 203–222
9. Havner, K.S. (1992) *Finite Plastic Deformation of Crystalline Solids*. Cambridge University Press
10. Bunge, H.J. (1993) *Texture Analysis in Material Science*. Cuviller Verlag Göttingen
11. Bertram, A. and Kraska, M. (1995) Description of finite plastic deformations in single crystals by material isomorphisms, Parker, D.F. and England, A.H. (eds.), *IUTAM Symposium on Anisotropy, Inhomogeneity and Nonlinearity in Solid Mechanics*, pp. 77–90
12. Sarma, G.B. and Dawson, P.R. (1996) Texture predictions using a polycrystal plasticity model incorporating neighbor interactions, *Int. J. Plast.* **12**(8), pp. 1023–1054
13. Kraska, M. and Bertram, A. (1996) Simulation of polycrystals using an FEM-based representative volume element, *Technische Mechanik* **16**(1), pp. 51–62

COMPUTATIONAL MICRO–MACRO–TRANSITIONS IN THERMOPLASTIC ANALYSIS AT FINITE STRAINS

C. MIEHE AND J. SCHRÖDER
Institut für Mechanik (Bauwesen) Lehrstuhl I
Universutät Stuttgart
D–70550 Stuttgart, Pfaffenwaldring 7

1. Introduction

We discuss aspects of the formulation and numerical implementation of homogenization methods for the simulation of macroscopic thermomechanical material response of heterogeneous materials. Homogenization approaches based on average theorems as outlined e.g. by Hill [2], Suquet [10], Bruhns [1], Nemat–Nasser and Hori [8] are recast into a straightforward computational procedure for micro–macro–transitions at large strains. The proposed concept is suitable for the numerical analysis of macroscopic phenomena of materials with complex microstructures, such as texture developments in metallic polycrystals or overall properties of granular and composite materials.

In this paper we focus on the simulation of metal thermoplasticity at finite strains. The underlying goal is a comparative study of different approaches to micro–macro–transitions in the context of the simulation of texture developments. Here, the basic concept is to endow the macroscopic continuum *locally* with a representative microstructure which represents a polycrystalline aggregate, i.e. a representative assembly of single crystal grains. The deformation of this microstructure is determined by the local deformation at a typical material point of the macro–continuum. The macroscopic extensive variables like the stresses and the dissipation are then defined as volume averages of their microscopic counterparts defined on the representative microstructure. In the computational procedure proposed here, we evaluate these averages in a straightforward manner. The

O.T. Bruhns and E. Stein (eds.),
IUTAM Symposium on Micro- and Macrostructural Aspects of Thermoplasticity, 137-146.

SOLID MECHANICS AND ITS APPLICATIONS
Volume 62

Series Editor: G.M.L. GLADWELL
Solid Mechanics Division, Faculty of Engineering
University of Waterloo
Waterloo, Ontario, Canada N2L 3G1

Aims and Scope of the Series

The fundamental questions arising in mechanics are: *Why?*, *How?*, and *How much?* The aim of this series is to provide lucid accounts written by authoritative researchers giving vision and insight in answering these questions on the subject of mechanics as it relates to solids.

The scope of the series covers the entire spectrum of solid mechanics. Thus it includes the foundation of mechanics; variational formulations; computational mechanics; statics, kinematics and dynamics of rigid and elastic bodies; vibrations of solids and structures; dynamical systems and chaos; the theories of elasticity, plasticity and viscoelasticity; composite materials; rods, beams, shells and membranes; structural control and stability; soils, rocks and geomechanics; fracture; tribology; experimental mechanics; biomechanics and machine design.

The median level of presentation is the first year graduate student. Some texts are monographs defining the current state of the field; others are accessible to final year undergraduates; but essentially the emphasis is on readability and clarity.

IUTAM Symposium on

Micro- and Macrostructural Aspects of Thermoplasticity

Proceedings of the IUTAM Symposium
held in Bochum, Germany,
25–29 August 1997

Edited by

O. T. BRUHNS
Institute of Mechanics,
Ruhr-University Bochum,
Germany

and

E. STEIN
Institute of Structural and Computational Mechanics,
University of Hannover,
Germany

KLUWER ACADEMIC PUBLISHERS
DORDRECHT / BOSTON / LONDON